The Role of Intergranular Regions in Sintered Nd-Fe-B Magnets with $(B.H)_{max}$ > 420 kJ/m^3 (52.5 MGOe)

J. Fidler, T. Schrefl, S. Sasaki*and D. Suess

Institute of Applied and Technical Physics, Vienna University of Technology, Wien, Austria
** Rare-earth dev., Showa Denko K.K., Saitama 369-1893, Japan*

Abstract

Anisotropic Nd-Fe-B magnets with a high remanence and energy density were produced by powder metallurgy. In order to obtain an energy density of $(B.H)_{max}$ > 420 kJ/m^3 a minimum coercive field of ${}_JH_c$>750 kA/m is necessary. Experimental investigations have shown that the improving alignment of the grains decreases the coercive field of the sintered magnets. It was found that abnormal grain growth preferentially occurs in magnets with a higher degree of misalignment. 3-dimensional micromagnetic simulations show that the intergranular region between the grains, which is determined by the composition of the magnets and the annealing treatment, plays a significant role determining the magnetic properties. The coercivity is determined by the long range dipolar interaction and short range exchange coupling between neighbouring grains. The numerical finite element simulations show that assuming a disturbed intergranular region of about 5 to 10 nm with a reduced magnetocrystalline anisotropy the calculated coercive field is reduced to comparable experimental values of ${}_JH_c$<1000 kA/m. The micromagnetic simulations further show that in the case of a reduced anisotropy between the hard magnetic grains the nucleation of reversed domains starts at the grain boundaries, and the coercive field increases with decreasing alignment of the hard magnetic grains in the range of 8° to 16° misalignment.

Introduction

Nd-Fe-B sintered magnets possessing outstanding magnetic properties have developed into a major permanent magnet material in the past 15 years since their invention. The drastic increase of the energy density product of newly developed $Nd_2Fe_{14}B$ based magnets enabled the invention of many new applications of permanent magnets. Applications of highest energy density magnets (> 400 kJ/m³), are expanding; voice coil motors for hard disk drives, magnetic resonance imaging, small sized motors, electrical devices and so on. These magnets are produced by a conventional powder metallurgical process which is essentially based on alloy-making, coarse-milling, pulverising, pressing in a magnetic field, sintering, heat-treatment and surface coating. In this process it is very important to keep the processing atmosphere either in a vacuum or in an inert gas, because rare earth elements easily oxidise.

The formation and distribution of the phases is determined by the composition of the magnets and the annealing treatment. High performance $Nd_2Fe_{14}B$-based permanent magnets are produced with different composition and various processing techniques [1,2], which influence the complex, multiphase microstructure of the magnets, such as grain size, the orientation of the easy axes of the grains and the distribution of phases. The grain size of sintered magnets which is in the order of several microns and the alignment of the grains strongly depend on the compacting sintering and annealing parameters.

Experimental results

Magnets of the composition $Nd_{15.1-x}Fe_{78+x}B_6Cu_{0.03}Al_{0.7}$ [x=0-2.5] were prepared by the powdermetallurgical sintering route [3]. The energy density product >400 kJ/m^3 and the coercive field of 800 kA/m were obtained after a combination of rubber isostatic and transverse die pressing methods under optimised sintering conditions. The misalignment of the hard magnetic grains with a diameter of 2~5 µm was calculated in the best case in the order < 14°. The high oxygen content of the magnets was gradually decreased from values of 4000 - 6000 ppm to a value < 1000 ppm. This high oxygen content was one limiting factor to decrease the Nd-content in order to improve the volume fraction of the hard magnetic phase. The demagnetisation curve of an optimised magnet with a low oxygen content and a composition of $Nd_{13.5}Fe_{bal}B_{5.95}Cu_{0.03}Al_{0.7}$ is shown in Fig.1. The magnets produced were sintered between 960°C and 1100°C. The sintering temperature was varied to get optimum density (7.5~7.6 g/cm^3) and $(B.H)_{max}$. The density of the samples and the remanence increased with increasing sintering temperature keeping the sintering time constant (3 hours), while the squareness of the demagnetisation curve only partly increased and drastically decreased as abnormal grain growth of the 2:14:1 grains occurred [4]. Abnormal grain growth (AGG) of the 2:14:1 grains occurred preferentially in magnets with low oxygen content. The oxygen content strongly affects the AGG and the magnets with higher oxygen content have the higher critical temperatures at which the AGG occurs. On the other hand, isotropic magnets tend to have the lower critical temperatures than anisotropic magnets by 10-20°C. A single or a two step (800°C plus quenching) annealing treatment at 500~600°C for 60 min increased the coercive field by about 200 kA/m or about 20%.. Even though too high oxygen content deteriorates magnetic properties, appropriate oxygen content works very effectively to prevent the AGG. In high oxygen containing magnets controlled oxidation occurs during jet milling and compaction on air and insufficient sintering atmosphere. No significant oxidation occurs after the jet milling process in low oxygen magnets.

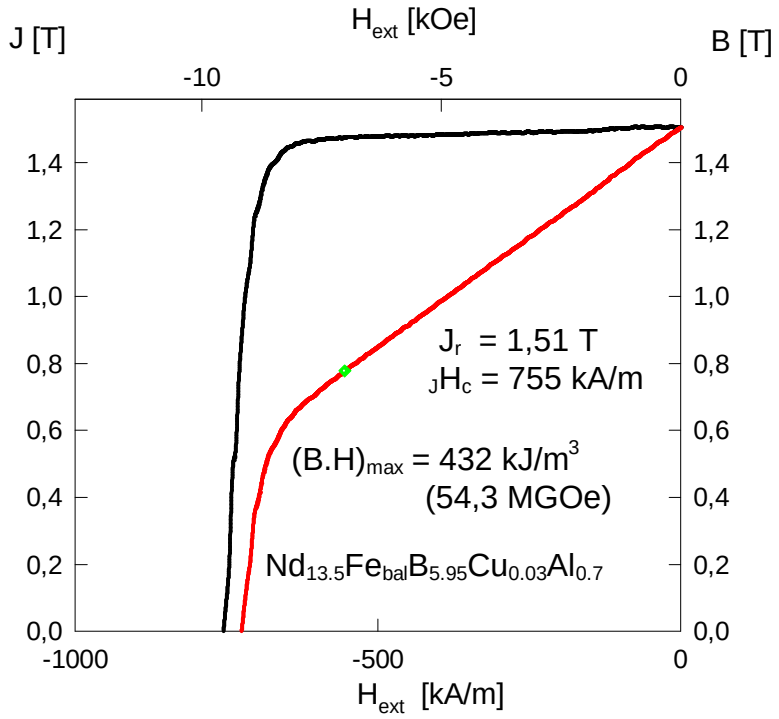

Figure 1: Demagnetisation curve of an optimised $Nd_{13.5}Fe_{bal}B_{5.95}Cu_{0.03}Al_{0.7}$ sintered magnet manufactured by a combination of rubber isostatic die and transverse die pressing.

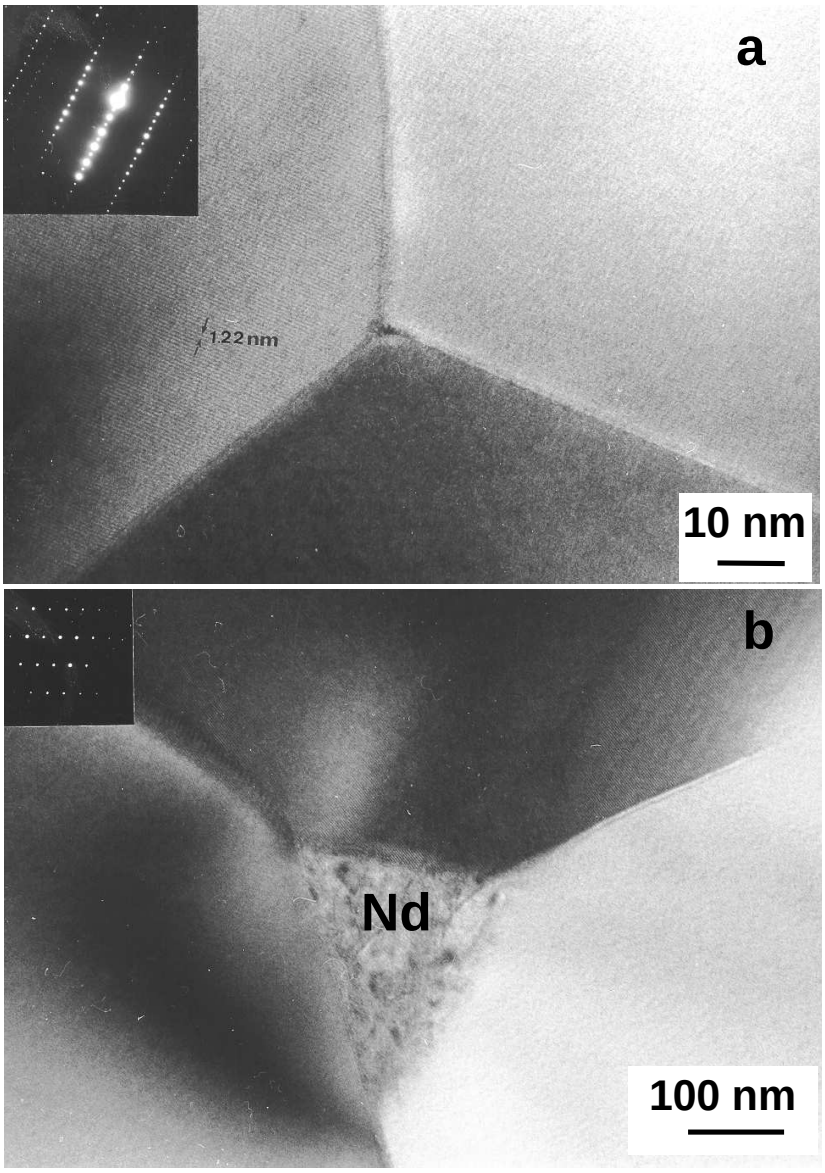

Figure 2: TEM image of grain boundary junctions of a $Nd_{13.7}Fe_{bal}B_{5.95}Cu_{0.03}Al_{0.7}$ sintered magnet with c-axis of grains is parallel (a) and perpendicular (b) to the image plane.

Remanence and energy product increase with decreasing Nd-content, whereas the coercive field shows its highest value at a high Nd-content. In the case when the oxygen content of the magnets was determined to be in the order of 4000 to 6000 ppm, a large part of the Nd was bound in the stable phase Nd_2O_3 phase. This is the why below 14 at.% Nd the density and the hard magnetic properties of the magnets drastically deteriorated in magnets with a high oxygen. A measured density and a theoretical spontaneous magnetisation give an estimated remanence, which also depends on the degree of alignment. Using the measured densities and remanences the J_s was calculated from the composition. In the case of $Nd_{13.5}Fe_{bal}B_{5.95}$, the volume fraction of the hard magnetic phase is estimated at 94.4 vol.%, which corresponds to J_s = 1.51 T at the full density. The remaining 5.6 vol.% consist of the $Nd_{1+\varepsilon}Fe_4B_4$ and other boron-rich phases, the Nd-rich intergranular phases, Nd_2O_3, pores and other additional phases. However, a certain amount of Nd-rich phase is necessary to get the appropriate ${}_JH_c$. The TEM investigation of high remanence and low Nd-content sintered magnets obtains Nd-rich phases only occasionally at grain boundary

junctions (Fig.2a and b). The lattice plane image corresponds to the (001) basal planes. The three grains are nearly parallel to each other and the diffraction pattern of the grains only changed slightly in the distribution of the intensity among the diffracting spots (Fig.2a). Correspondingly a sluggish contrast of the same (001) planes is seen in the upper right grain and a still fainter basal plane lattice contrast is seen in the lower grain. The misalignment between the three grains is calculated to be less than 5°. The microstructure of the magnet did not significantly change when observed with the c-axis perpendicular to the sample plane. The fibre-texture along [001] is observed and misalignments of the <100> directions in neighbouring grains was measured to be in the order of 20-25° (Fig.2b). The TEM observation agrees with the x-ray global texture measurements.

Nd-Fe-B magnets with high remanence and highest energy density

The theoretical maximum value of the energy density product is in the case of a perfectly squared demagnetisation curve given by:

$$(B \cdot H)_{\max}^{theor.} = \frac{1}{4 \cdot \mu_0} \cdot J_r^2 = \frac{1}{4 \cdot \mu_0} \cdot \left(J_s \cdot \frac{\rho}{\rho_0} \cdot V_{hm} \cdot \cos\varphi \right)^2 \quad \text{if} \quad \left| {}_J H_c \right| \geq \frac{1}{2 \cdot \mu_0} \cdot J_r \qquad (1)$$

where, J_s is the saturation magnetisation of the hard magnetic phase (1.61 T), V_{hm} and φ are the volume fraction and the degree of alignment of the hard magnetic grains, respectively. In order to enhance J_r and therefore the energy density product, it is necessary to avoid pores and to densify the magnets up to the theoretical value, increase the volume fraction V_{hm} and achieve a high degree of alignment φ. The theoretical value of the maximum energy product of $Nd_2Fe_{14}B$ based magnets is calculated to be 512 kJ/m³ assuming 100% perfect alignment and 100% volume fraction of the hard phase. The origin of this magnetic property lies in the $Nd_2Fe_{14}B$ ternary tetragonal compound as a main phase. In addition, according to the ternary Nd-Fe-B phase diagram this magnet contains also a certain amount of a Nd-rich phase, which is essential for sintering with liquid phase. In order to densify the magnets up to the theoretical density, it is very important to control the composition of magnets thus generating sufficient amount of liquid phase at sintering.

Intergranular phases change the coupling behaviour between the hard magnetic grains. Disturbed regions and non magnetic phases between the grains eliminate the direct exchange interaction and also reduce the long-range magnetostatic coupling between the hard magnetic grains. Both effects lead to an increase of the coercive field. Several authors have reported to obtain Nd-Fe-B based magnets with 400 kJ/m^3 energy density product by keeping the oxygen content low [5], using the powder mixing technique [6], increasing the magnetising field and reducing the pressure during compaction [7]. The rubber isostatic pressing (RIP) technique has been developed by Sagawa et al. [8,9] to improve the orientation of the particles in the green compact to obtain sintered magnets with perfect orientation. In the conventional die pressing the pressure applied to the powder is uniaxial. The uniaxial pressure tends to disturb the orientation of the particles during the pressing. To prevent this orientation disturbance, the powder has to be subjected to a strong magnetic field throughout the pressing. One possibility to improve the alignment factor is to optimise the alignment field and/or pressure during transverse pressing. Even the sintering process influences the degree of alignment of the grains [10]. On the other hand several authors [9,11] found that the highest alignment is obtained by isostatic die pressing (φ=11-14°), followed by the transverse field die pressing (φ=18-20°)and the axial field die pressing (φ=25-27°).

Micromagnetic simulation of magnetisation reversal at grain boundaries

The coercive field is determined by the long range dipolar interaction and short range exchange coupling between neighbouring hard magnetic grains. The doping of elements changes the phase relation and favours the formation of new phases. Additional secondary non-magnetic intergranular phases decrease the remanence and interrupt the magnetic interactions between the grains, thereby improving the coercivity of large grained sintered magnets. For magnets with higher Nd-concentrations grain size, misorientation and distribution of grains control coercive field. Numerical micromagnetics help to understand the correlation between the intrinsic magnetic properties, the microstructure and the magnetic interaction that determines coercivity and remanence. The dipolar interactions considerably reduce the coercive field of ideally oriented particles with respect to ${}_{J}H_c$ of an isolated particle. Exchange coupling between misaligned grains drastically reduces the coercive field in nanocrystalline magnets. The higher the Nd-content of the magnet and therefore the volume fraction of the Nd-rich intergranular phase is, the more reduced is the contribution of the exchange and also dipolar coupling between the grains. In magnets with high remanence and energy product the decrease of the volume fraction of the hard magnetic phase by doping of elements by the formation of secondary phases has to be avoided. For technological reasons an average misorientation to the to the alignment direction of the magnet occurs. Finite element simulations reveal the influence of the intergranular phase and the misorientation of the hard magnetic grains on the complex magnetisation reversal process.

The hysteresis properties either follow from the direct minimization of the total magnetic Gibb's free energy or from the time integration of the Gilbert equation of motion The numerical simulation starts form the total magnetic Gibb's free energy E_t which is the sum of the sum of the exchange, the magneto-crystalline anisotropy energy, the magnetostatic energy, and the Zeeman energy of the magnetic polarization in an external field $\boldsymbol{H}_{\text{ext}}$ [12]:

$$E_t = \int \left[A \sum_{i=1}^{3} \left(\nabla \beta_i\right)^2 - K_1 (\mathbf{J} \cdot \mathbf{u})^2 - \frac{1}{2} \mathbf{J} \cdot \mathbf{H}_d - \mathbf{J} \cdot \mathbf{H}_{\text{ext}} \right] dV \qquad (2)$$

where A is the exchange constant, $\boldsymbol{H}_d$ is the demagnetizing field, K_1 is anisotropy constant, and $\boldsymbol{u}$ denotes the unit vector parallel to the c-axis. When the direction cosines of the magnetization β_i are approximated by piecewise linear functions on the finite element mesh, the energy functional (3) reduces to an energy function with the nodal values of the direction cosines as unknowns. Its minimization of with respect to the direction cosines of the magnetization at the nodal points variables, subject to the constraint $ß_1^2 + ß_2^2 + ß_3^2 = 1$, provides an equilibrium distribution of the magnetization. To satisfy the constraint, the magnetization can be represented by polar coordinates. The resulting algebraic minimization problem is solved using a quasi-Newton conjugate gradient technique. The demagnetising field $\mathbf{H}_d$ follows from the magnetic scalar potential which is calculated using a hybrid finite element / boundary technique [13].

The numerical minimization method determines the path the system proceeds towards the local minimum. The Gilbert equation

$$\frac{\partial \mathbf{J}}{\partial t} = -|\gamma| (\mathbf{J} \times \mathbf{H}_{\text{eff}}) + \frac{\alpha}{J_s} \left(\mathbf{J} \times \frac{\partial \mathbf{J}}{\partial t} \right) \qquad (3)$$

is assumed to give the physical path of the system towards equilibrium. The effective field, $\mathbf{H}_{\text{eff}} = \delta E_t / \delta \mathbf{J}$ is the variational derivative of the magnetic Gibb's free energy. A Gilbert damping constant $\alpha = 1$ was used. Equations (3) or (4) are solved using standard finite element techniques. The numerical details are given in [14-16].

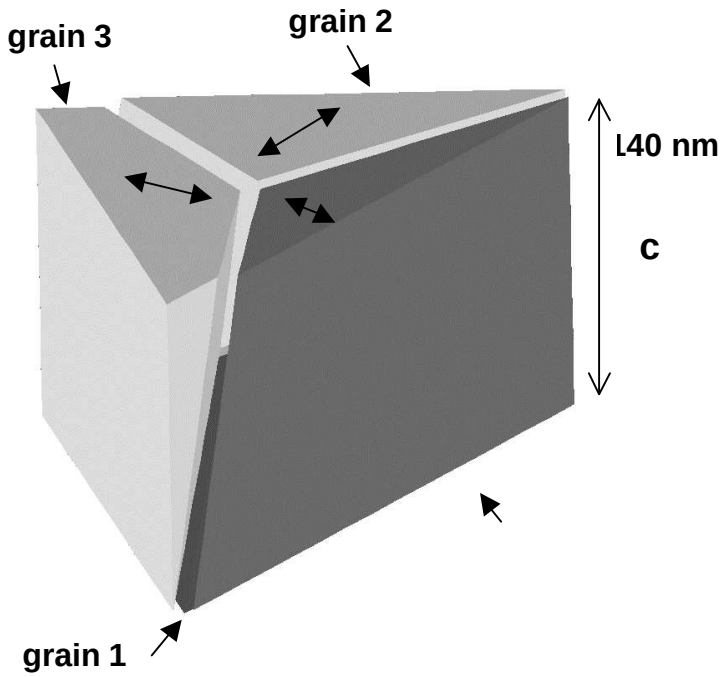

Figure 3: 3D grain structure model with intergranular region near the junction of four neighbouring grains. For the calculations, the misalignment of the grains was varied from 8° to 16° from the alignment direction c.

Micromagnetic 3D finite element calculations were used to simulate the influence of Nd-rich phases located at grain boundary junctions, reduced anisotropy near the grain boundaries, and the degree of alignment on the nucleation of reversed domains. The numerical results show that all three effects are correlated and contribute in a complex way to the measured coercivity. The finite element model used for the simulations are based on TEM investigations. The TEM micrographs of Fig.2 show the grain junction of three grains and a small amount of Nd-rich intergranular phase. In order to avoid long computation times a region close to the grain intersection of four grains was chosen. Different crystallographic orientations are assigned to each grain. In addition, the grains are partly separated by an narrow intergranular phase of a thickness in the order of 5 to 10 nm. Once the polyhedral grain structure is obtained, the grains are further subdivided into tetrahedral finite elements. The 3D drawing of Fig.3 shows schematically the corresponding model of the microstructure which is used for the simulations. Close to the grain boundary junction the misaligned hard grains are separated by the intergranular region. The four grains are drawn separately for a better presentation. The arrows in the middle of the upper grain surfaces represent the projection of the easy axis onto the image plane.

Figure 4 shows the 3D model of the finite element model and the generated mesh near the junction of four neighbouring grains. The dark regions shows the dispersion of Nd-rich phases. The anisotropy constant is varied in the intergranular regions which are drawn dark in Fig. 4. For the calculations the material parameters of the $Nd_2Fe_{14}B$ phase at T = 300 K were taken from Sagawa et al. [17] (K_1 = 4.5 10^6 J/ m^3, J_s = 1.61 T, A = 12.5 pJ/m). For the calculations, the average misalignment of the $Nd_2Fe_{14}B$ grains was varied from 8° to 16°. The difference in the intrinsic magnetic properties between the bulk of the grains and the grain boundary region is taken into account. Various transitions of the intrinsic parameter from one grain to the neighbouring grain s are possible.

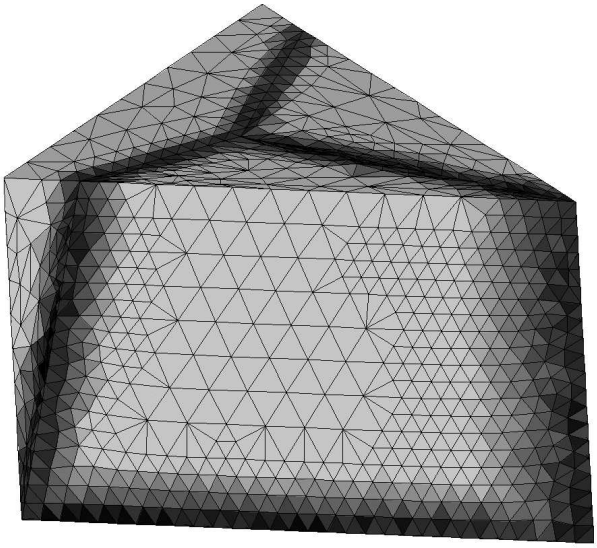

Figure 4: Discretization of the grain boundary junction model into finite elements. In the dark intergranular regions the intrinsic properties are varied.

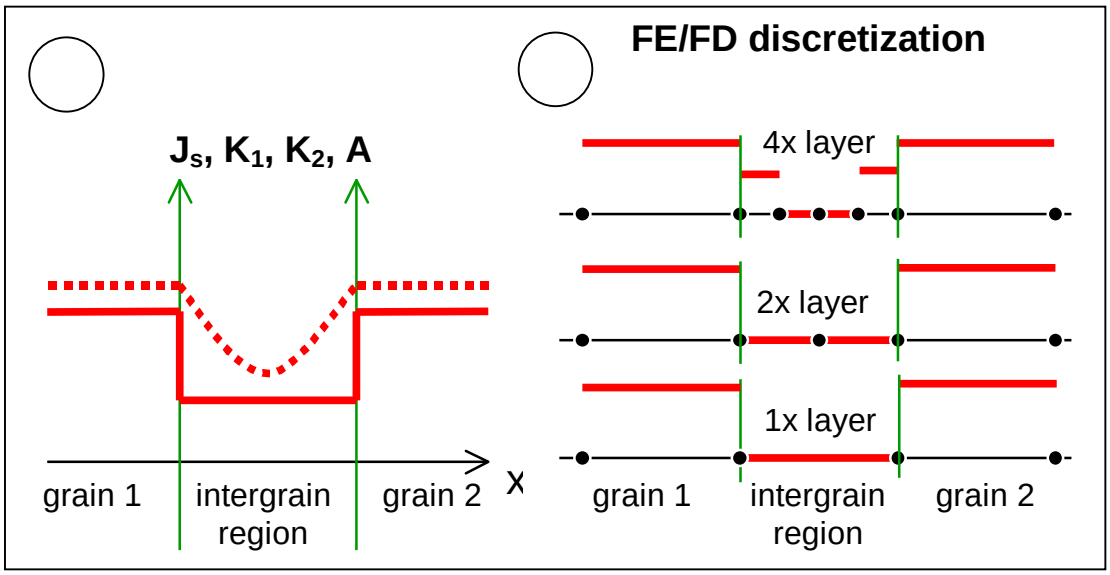

Figure 5: Schematic 1D transition of the intrinsic parameters in the intergranular region.

Figure 5 shows a one dimensional model of the discontinuous and continuous transitions (Fig.5a) and the linear transition model by inserting additional elements in the intergranular region in the finite element or finite difference models (Fig.5b).

Perfect grain boundaries

For a perfect microstructure the numerical results agree well with the Stoner-Wohlfarth theory [18]. The most misoriented grain, which has the largest angle between the c-axes and the alignment direction, determines the coercive field. The coercive field decreases with increasing misalignment.

Distorted grain boundaries

A reduction of the magneto-crystalline anisotropy near the grain boundaries leads to a linear decrease of the coercive field. The coercive field decreases from about 3800 kA/m to 1200 kA/ m

as the anisotropy constant in a 10 nm thick region near the grain boundaries is reduced from its bulk value to zero. The demagnetisation curves of Fig.6 compare perfect grain boundaries, distorted grain boundaries and experimental data. The influence of the magnetocrystalline anisotropy of the intergranular region on the coercive field is clearly shown. The reduction in the magneto-crystalline anisotropy reverses the dependence of the coercive field on the degree of alignment. The coercive field increases by about 80 kA/m as the misalignment angle is changed from 8° to 16°, if $K_1^{inter} < 0{,}4\ K_1^{bulk}$ (Fig.7). This effect has to be attributed to a higher demagnetising field in the well aligned sample which initiates the nucleation of reversed domains within the defect region.

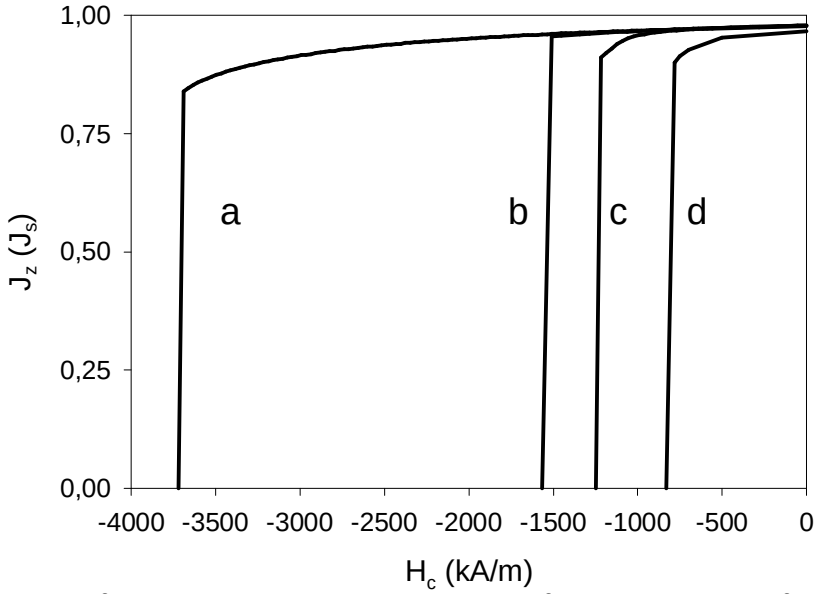

Figure 6: Comparison of simulated demagnetizing curves of magnets with perfect grain boundaries and distorted grain boundaries with experimental data a) K1 = K1, b) K1 = K1 linear, c) K1 = 0, d) experiment

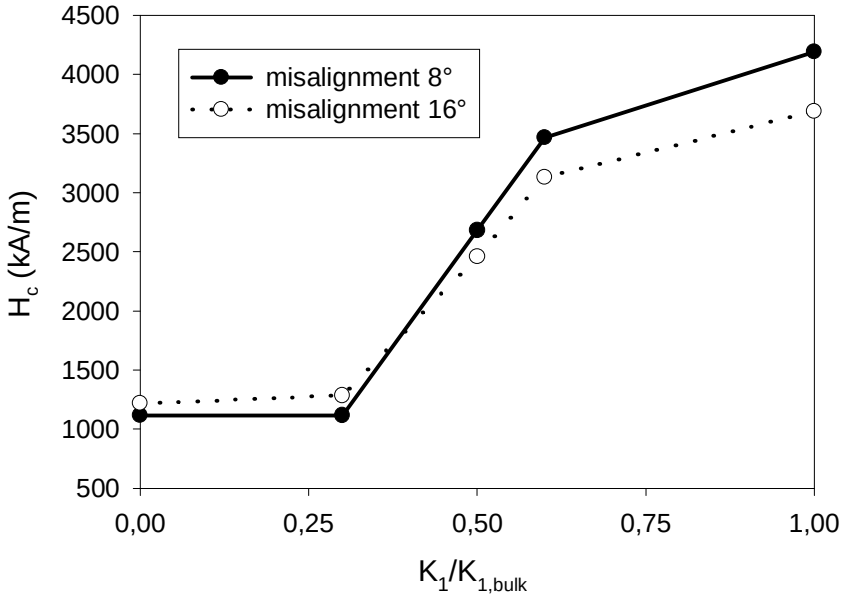

Figure 7: The reduction in the magneto-crystalline anisotropy reverses the Stoner-Wohlfarth dependence of the coercive field on the degree of alignment.

The comparison with experimental data provides a detailed understanding of magnetization reversal in high energy density permanent magnets. The simulations explain experimental data [19] which show a decrease of the coercive field with increasing misalignment for high-coercive, Dy-containing Nd-Fe-B magnets, whereas a slight increase of coercivity with misalignment is observed in Dy-free Nd-Fe-B magnets. The simulations allow to identify the regions within the microstructure where reversed domains are nucleated (Fig.8). The isosurfaces show the growth of the reversed domains as a function of the applied field.

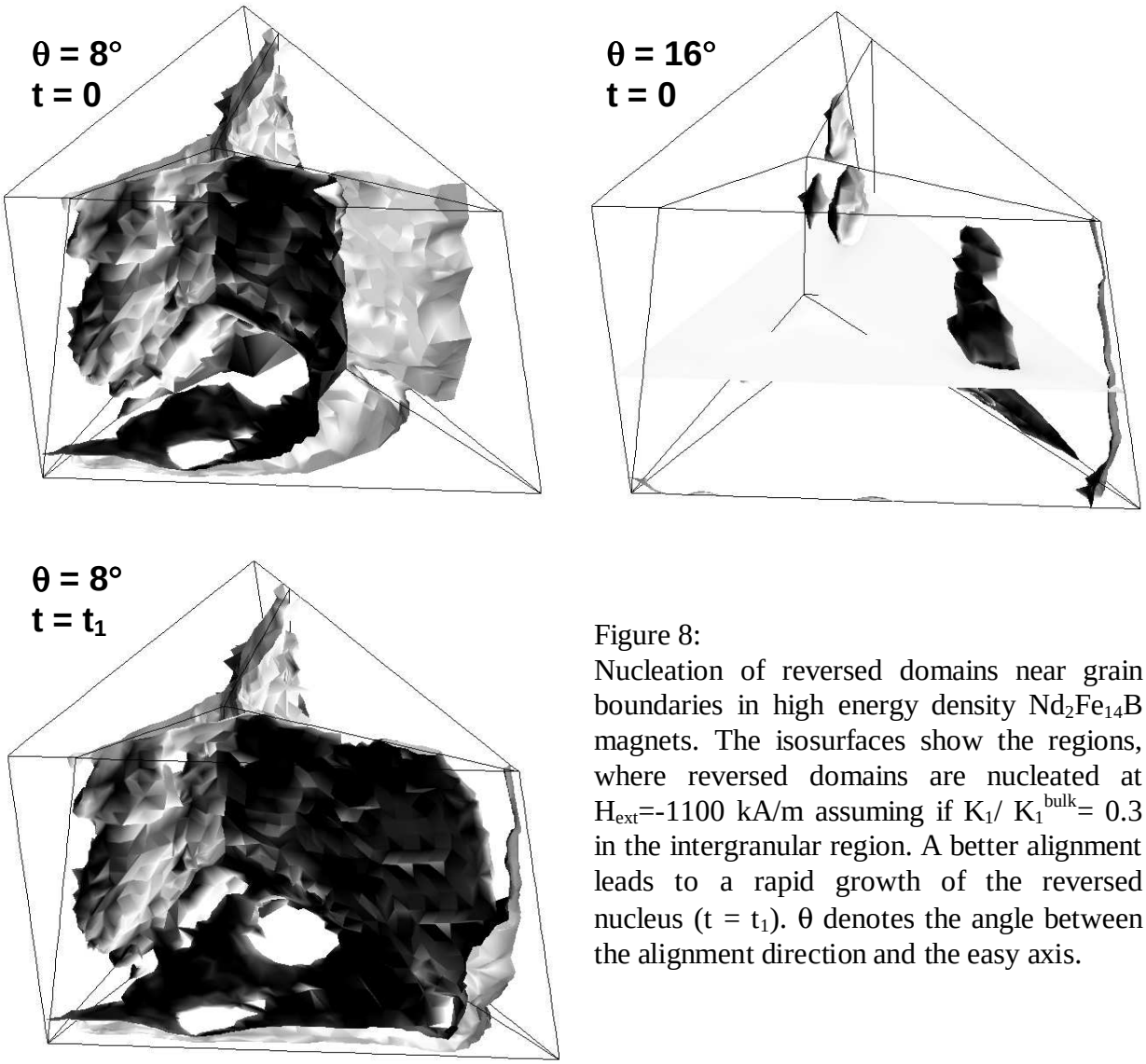

Figure 8:
Nucleation of reversed domains near grain boundaries in high energy density $Nd_2Fe_{14}B$ magnets. The isosurfaces show the regions, where reversed domains are nucleated at H_{ext}=-1100 kA/m assuming if K_1/ K_1^{bulk}= 0.3 in the intergranular region. A better alignment leads to a rapid growth of the reversed nucleus ($t = t_1$). θ denotes the angle between the alignment direction and the easy axis.

Nd-rich boundary phases

The coercive field of Nd-Fe-B sintered magnets increase with increasing Nd content [20]. The finite element simulations confirm that non-magnetic Nd-rich phases on grain boundary junctions significantly increase the coercive field. The simulations show that the coercive field increases by about 15% as non magnetic Nd-rich phases near grain boundary junctions are taken into account. The presence of the Nd-rich phase significantly changes the exchange and the magnetostatic interactions. As a consequence the nucleation of reversed domains is suppressed.

It should be mentioned that it is extremely difficult to compare the dependence of the coercivity of sintered Nd-Fe-B magnets on the alignment coefficient, since the optimum sintering conditions change with the degree of alignment.

Conclusions

The quantitative interaction between magnetisation and microstructure has been calculated by means of a micromagnetic finite element technique. Our micromagnetic simulations of the magnetization reversal process revealed exact predictions of the influence of intergranular phases on the coercive field: Nd-rich phases at grain boundary junctions reduce the effective coupling between the grains an thus increase the coercive field up to 15 percent. Perfect grains without any reduction of the magnetocrystalline anisotropy show a behaviour which is expected from the Stoner-Wohlfarth theory. The coercive field decreases with increasing misalignment. Defects at the surface reduce the magnetocrystalline anisotropy locally and thus drastically decrease the coercive field. Then the coercive field shows only weak dependence on the degree of alignment. The defects change the local effective fields and thus reverse the behaviour observed for perfect grains: A better alignment slightly reduces the coercive field.

Acknowledgement

This work is supported by the Austrian Science Fund projects FWF P13433 and Y132-PHY.

Literature

[1] J.F. Herbst and J.J. Croat, *JMMM* **100** (1991) 57.
[2] J. Fidler and T. Schrefl, *JAP* **79** (1996) 5029.
[3] S. Sasaki, PhD Thesis, Vienna University of Technology, Austria, 1999.
[4] W. Rodewald, B. Wall and W. Fernengel, *IEEE Trans. Magn.* **33** (1997) 3841.
[5] M. Sagawa, S. Hirosawa, H. Yamamoto, S. Fujimura and Y. Matsuura, *Jpn. JAP* **26** (1987) 785.
[6] E. Otsuki, T. Otsuka and T. Imai, *Proc. 11th Int. Workshop on rare earth magnets and their applications*, Pittsburgh, ed. by Shankar, Vol.1, (1990) 328.
[7] M. Endoh and M. Shindo, *Proc. 13th Int. Workshop on rare earth magnets and their applications, Birmingham*, ed. by Manwaring et al, Vol.1, (1994) 397.
[8] M. Sagawa and H. Nagata, *IEEE Trans Magn*. **29** (1993) 2747.
[9] M. Sagawa, H. Nagata O. Itatani and W. Watanabe, *Proc. 13th Int. Workshop on rare earth magnets and their appl.*, Birmingham, ed. by Manwaring et al, Suppl., 1994, 13.
[10] T.S. Chin, M.P. Hung, D.S. Tsai, K.F. Wu and W.C. Chang, *JAP* **64** (1988) 5531.
[11] W. Fernengel, A. Lehnert, M. Katter, W. Rodewald and B. Wall, *JMMM* **157/158** (1996) 19.
[12] W. F. Brown Jr., Micromagnetics (Wiley, New York, 1963).
[13] D. R. Fredkin and T. R. Koehler, *IEEE Trans. Magn*. **26** (1990) 415.
[14] T. Schrefl and J. Fidler, *JMMM* **177** (1998) 970.
[15] T. Schrefl, H. Roitner, and J. Fidler, *JAP* **81** (1997) 5567.
[16] T. Schrefl, J. Fidler, K. J. Kirk and J. N. Chapman, *IEEE Tr.. Magn*. **33** (1997) 4182.
[17] M. Sagawa, S. Fujimura, H. Yamamoto, Y. Matsuura, and S. Hirosawa, *JAP* **57** (1985) 4094.
[18] E. C. Stoner and E. P. Wohlfarth, *Philos. Trans. R. Soc.* **240** (1948) 599.
[19] A.S. Kim, F.E. Camp and H.H. Stadelmaier, *JAP* **76** (1994) 6265.
[20] S. Hirosawa and Y. Kaneko, *Proceedings 15th Int. Workshop on Rare-Earth Magnets and theirApplication*, Dresden, Germany, 1998, 43.